Dalton Transactions

Accepted Manuscript

ROYAL SOCIETY OF CHEMISTRY

www.rsc.org/dalton

Cite this: DOI: 10.1039/c0xx00000x

www.rsc.org/xxxxxx

ARTICLE TYPE

Mitochondrial selectivity and remarkable photocytotoxicity of a ferrocenyl neodymium(III) complex of terpyridine and curcumin in cancer cells†

Tukki Sarkar,[a] Samya Banerjee,*[b] Sanjoy Mukherjee [b] and Akhtar Hussain*[a]

Received (in XXX, XXX) Xth XXXXXXXXX 20XX, Accepted Xth XXXXXXXXX 20XX
DOI: 10.1039/b000000x

A series of four novel neodymium(III) complexes of formulation [Nd(R-tpy)(*O*-*O*)$(NO_3)_2$] (**1**–**4**), where R-tpy is 4′-phenyl-2,2′:6′,2″-terpyridine (Ph-tpy; **1**, **2**) and 4′-ferrocenyl-2,2′:6′,2″-terpyridine (Fc-tpy; **3**, **4**); *O*-*O* is the conjugate base of acetylacetone (Hacac; **1**, **3**) or curcumin (Hcurc; **2**, **4**) is synthesized and characterized. The single crystal structure of **1** shows that the complexes are discrete mononuclear species with Nd(III) centre in a nine coordinate environment provided by a set of O_6N_3 donor atoms. Complexes **1** and **3** having the simple acac ligand are prepared as control compounds. Complex **4**, possessing an appended ferrocenyl (Fc) and the curcumin moiety, is remarkably photocytotoxic to HeLa and MCF-7 cancer cells in visible light giving respective IC_{50} values of 0.7 μM and 2.1 μM while being significantly less toxic to MCF-10A normal cells (IC_{50} = 34 μM) and in the dark (IC_{50} > 50 μM). The phenyl appended complex **2**, lacking a ferrocenyl moiety, is significantly less toxic to both the cell lines when compared with **4**. Complexes **1** and **3,** lacking the photoactive curcumin moiety, do not show any apparent toxicity both in the light and dark. The cell death is apoptotic in nature and is mediated by the light-induced formation of reactive oxygen species (ROS). Fluorescence imaging experiment with HeLa cells reveals mitochondrial accumulation of complex **4** within 4 h of incubation. The complexes bind to calf thymus (ct) DNA with moderate affinity giving K_b values in the range of 10^4-10^5 M^{-1}. The curcumin complexes **2** and **4** cleave plasmid supercoiled DNA to its nicked circular form in visible light *via* $^1O_2$ and $^{\bullet}OH$ pathways. The presence of the ferrocenyl moiety is likely to be responsible for the enhanced cellular uptake and photocytotoxicity of complex **4**. Thus, the mitochondria targeting complex **4**, being remarkably cytotoxic in light but non-toxic in dark and to normal cells, is a potential candidate for photochemotherapeutic applications.

Introduction

Photodynamic therapy (PDT) is a clinically attractive chemotherapeutic modality for the treatment of cancer. In PDT, a photoactivable drug is administered to a cancer patient and the target tissue is irradiated with specific light in the presence of molecular oxygen thereby resulting in the generation of cytotoxic molecular species.[1,2] PDT has many advantages over conventional cancer therapies such as its low systemic toxicity, selective drug action within the photo-irradiated regions, low level of invasiveness and ability to overcome drug resistance.[1-6] Photofrin® is currently the FDA approved and clinically frequently prescribed organic PDT drug.[7,8] Unfortunately, the limitations such as skin sensitivity and hepatotoxicity associated with Photofrin® have prompted chemists to look for its alternatives.[8] Consequently, the light-activatable metal complexes of non-porphyrinic ligands have emerged as potential candidates in the PDT of cancer.[9-12] Metal complexes can provide variable coordination geometries, versatile spectral and redox properties and can cause cell death via photo-redox and/or type-I pathways besides generating cytotoxic singlet oxygen species in a type-II process.[9–12]

There is currently a growing interest in the coordination chemistry of lanthanides because of their promising applications in medicinal chemistry.[13-16] The most important application of lanthanides is the use of gadolinium(III) complexes such as Magnevist™ and Dotarem™ as clinical MRI contrast agents.[15] Although several transition metal-based PDT agents have been studied, the studies on lanthanide (Ln) complexes as PDT agents are rare apart from a few lanthanide complexes of macrocyclic and non-macrocyclic organic dyes.[17-2] The lutetium(III) texaphyrin (LUTRIN®) complex, for example, is known to show

[a] *Department of Chemistry, Handique Girls' College, Guwahati 781001, Assam, India. E-mail: akhtariisc@gmail.com; Tel: +91-361-2543793*
[b] *Department of Inorganic and Physical Chemistry, Indian Institute of Science, Bangalore560 012, Karnataka, India. E-mail: samya@ipc.iisc.ernet.in; Tel: +91-80-22932240.*

† Electronic supplementary information (ESI†) available: Reaction schemes, ESI-MS spectra, UV-visible spectra, cyclic voltammograms, packing diagrams, DFT structures and tables, stability and MTT assay plots, DNA gel electrophoresis diagrams. See DOI: 10.1039/b000000x/

promising PDT effect in the near-IR light.[21] The Ln(III) complexes with their poor stereochemistry and high coordination numbers can be appropriately designed by employing photosensitizing organic ligands possessing hard *O* and *N* donor atoms to achieve remarkable photocytotoxicity against cancer cells. Furthermore, such complexes could be non-toxic in the absence of light since the Ln(III) ions are redox inactive thereby making them desirable for cellular applications in the presence of reducing glutathione or ascorbic acid present in cells. Besides, the photoexcited lanthanide complexes can undergo facile intersystem crossing (ISC) due to the heavy atom effect induced by the heavy lanthanide cation thereby resulting in efficient generation of singlet oxygen.[22]

Bioorganometallics is an emerging area of research in medicinal chemistry.[23-25] Ferrocene and its conjugates have received considerable attention because they are known to possess many medicinal properties as antibacterial, antimalarial and antitumor agents.[23-25] Ferrocene conjugates have found their most promising application in the treatment of breast cancer. Around 66% of the breast cancers are hormone dependent where the estrogen receptor (ER+) is involved. The ferrocene moiety offers a number of advantages such as its stability in the physiological medium, lipophilicity, redox activity and nontoxic nature in the dark.[26] For example, the ferrocene appended anticancer drug tamoxifen is known to show enhanced activity against both hormone dependent (ER+) and hormone independent (ER-) breast cancers.[27] Similarly, ferroquine, the ferrocene conjugated antimalarial drug chloroquine, is significantly more active than chloroquine.[28] In addition to the ferrocene derivatives, the ruthenium-arene and ruthenium-cyclopentadienyl half-sandwich complexes are known as organometallic antitumor agents. The water-soluble ruthenium(II)-arene-pta (RAPTA) complexes have shown promising results as anti-metastatic agents.[23-25] The ferrocenium ion itself is known to show cytotoxic activity.[23] While the ferrocene appended oxovanadium(IV) and copper(II) complexes have been studied as photocytotoxic agents, the lanthanide complexes are virtually unexplored.[29-31] Our interest to design ferrocene based photocytotoxic agents is based on the effectiveness of bioorganometallic complexes as promising drug candidates showing enhanced selectivity and anticancer activity.

Curcumin (Hcurc) and its metal complexes have received a great deal of current attention because curcumin shows a number of of medicinal properties.[32,33] Curcumin (bis(4-hydroxy-3-methoxyphenyl)-1,6-diene-3,5-dione, Hcurc) is a naturally occurring *β*-diketone compound present in the herb *Curcuma longa* L. It is known to be a potent anticancer agent and cause apoptosis selectively in cancer cells while being harmless to the normal cells.[33,34] However, the poor bioavailability and pharmacokinetic profile of curcumin has severely limited its usefulness as drug despite its broad spectrum of biological activities.[34,35] Therefore, several derivatives of curcumin have been studied to circumvent its drawbacks.[36-38] One of the subtle and successsful strategies takes advantage of curcumin's metal coordinating ability.[36-38] Although, there are reports on the anticancer activity of curcumin and its metal complexes, the studies on the photodynamic potential of its metal complexes, especially with Ln(III), are still rare despite its rich photophysical and photochemical properties and ability to induce PDT effect.[39-44] The green fluorescence emission of curcumin, moreover, offers a convenient means to study the localization of the curcumin complexes in cancer cells.[41-46]

Although nucleus is the prime target of most anticancer drugs, there is currently increasing interest in search for compounds that target cell organelles other than the nucleus because of the limitations associated with the nucleus targeting drugs.[47,48] The resistance of cancer cells to cisplatin, for instance, is due to the extensive repair of the cisplatin-DNA adducts by the nucleotide excision repair (NER) pathway.[49] Drugs that selectively target mitochondria, for instance, can serve as potential anticancer agents because mitochondria perform key cellular functions and any inhibition with their functions can lead to apoptosis.[47,48,50] Besides, mitochondria do not possess a functional nucleotide excision repair mechanism to repair DNA adducts. Therefore, mitochondria targeting drugs are highly desirable for successful chemotherapeutic applications. For example, the FDA approved clinical PDT drug Photofrin® is known to target the mitochondria of cancer cells and cause apoptosis in tumour cells.[51] Although, oxovanadium(IV) and cobalt(III) complexes showing mitochondrial selectivity are known, the reports on lanthanide complexes are virtually unknown .[43,44]

Very recently, we have reported Co(III) and Fe(III) complexes of curcumin showing photocytotoxicity against cancer cells in visible light.[44,45] The present work results from our effort to study lanthanide complexes of curcumin as photocytotoxic agents. Herein, we present the studies on the in vitro photodynamic potential of a series of neodymium(III) (Nd(III)) complexes. Nd(III) was chosen as the representative lathanide. Nd(III) complexes have earlier been studied as cytotoxic agents.[52] The Nd(III) complexes of acetylacetone (Hacac) have been prepared as controls to understand the role of curcumin (Fig. 1). We have synthesized and characterized four new lanthanide(III) complexes of formulation [Nd(R-tpy)(*O*-*O*)$(NO_3)_2$] (**1**–**4**), where R-tpy is a *N,N,N*-donor terpyridine ligand, viz., 4′-phenyl-2,2′:6′,2″-terpyridine (Ph-tpy; **1**, **2**) and 4′-ferrocenyl-2,2′:6′,2″-terpyridine (Fc-tpy; **3**, **4**); *O*-*O* is the monoanion of acetylacetone (Hacac; **1**, **3**) or curcumin (bis(4-hydroxy-3-methoxyphenyl)-1,6-diene-3,5-dione, Hcurc; **2**, **4**), and evaluated their photo-induced cytotoxicity in HeLa and estrogen ependent (ER+) MCF-7 cancer cell lines. While HeLa represents a model of highly proiferative cancer cell, the MCF-7 cell line is particularly suitable to study the cytotoxicity of ferrocence conjugates.[23-28] Significant results of this study include: (i) the remarkable photocytotoxicity of complex **4** in visible light with negligible toxicity in dark and to normal cells, (ii) the enhancement in photocytotoxicity of complex **4** compared to complex **2** due to the presence of the ferrocenyl moiety, (iii) the apoptotic mode of cell death due to the photo-assisted generation of intracellular ROS, (iv) the mitochondrial localization of complex **4** thereby making the cytosolic organelles as the potential targets, and (v) efficint visible light-triggered DNA cleavage activity.

[Space for Fig.1]

Results and discussion

Synthesis and general aspects

The complexes [Nd(R-tpy)(*O*-*O*)$(NO_3)_2$] (**1**–**4**) were synthesized in ~78% yield by a general two-step procedure in which the precursor complex, [Nd(R-tpy)$(NO_3)_3$], prepared by reacting $Nd(NO_3)_3.6H_2O$ with either Ph-tpy or Fc-tpy was reacted with either Hacac or Hcurc in methanol-acetonitrile binary solvent mixture (Fig. 1, Figs. S1, S2, ESI†). Because the Hacac and Hcurc ligands usually coordinate to metal ions as monoanions, their deprotonation was achieved by using triethylamine as the base. The elemental analyses data on the complexes were in good agreement with the theoretically calculated values. The FT–IR spectra of the complexes recored in pure solid phase displayed IR bands at 1595, 1490 and 1395 cm^{-1} corresponding to the C=O, C=C (β-diketonate) and NO_3^- stretching vibrations, respectively, indicating bidentate coordination mode of the β-diketonate (acac or curc) and NO_3^- ligands.[53] In addition, the complexes **2** and **4**, having the curc ligand showed an additional band at ~3390 cm^{-1} due to the phenolic hydroxyl groups of the curc ligand (Table 1). This value suggests that the phenolic –OH group is interacting with the neighboring $–OCH_3$ group of the curcumin ligand through hydrogen bonding.[53] The molar conductivity (Λ_M) measurements carried out in DMF (*N*,*N*-dimethyl formamide) suggested that all the complexes were 1:1 electrolytes corresponding to the dissociation of one nitrate ligand from the complex in solution (Table 1).[54] This observation is further supported by the ESI-MS measurements on the complexes in aqueous methanol showing the presence of a prominent $[M\text{-}(NO_3^-)]^+$ peak resulting from release of one nitrate anion (Figs. S3–S6, ESI†**)**. Thus, the solution formulation of the complexes could be [Nd(R-tpy)(*O*-*O*)(NO_3)]NO_3.[55] The electronic absorption spectra of complexes recorded in aqueous DMF showed a common absorption band around 275 nm assignable to a $\pi - \pi^*$ transition (Fig. 2(a), Figs. S7, ESI†).[44] In addition, the complexes **2** and **4** showed an intense curcumin-based visible absorption band within 400-500 nm originating from a $\pi \rightarrow \pi^*$ transition.[44] This absorption band can be exploited to study the visible-light triggered cytotoxicity of the complexes against cancer cells. The fluorescence emission spectra of complexes **2** and **4** measured in DMF showed a curcumin-based emission band centered at 525 nm with quantum yield (ϕ) value of ~ 0.01 when excited at 420 nm (Fig. 2(a)). This green emission from the complexes can be exploited to study their localization in cancer cells.[41-45] The solution susceptibility measurements of the complexes gave magnetic moments (μ_{eff}) in the range 3.56–3.62μ_B corresponding to the $[Xe]f^3$ configuration of Nd(III) center. The redox properties of the complexes were studied by electrochemical cyclic voltammetry measurements carried out in DMF in the presence of 0.1M tetrabutylammonium perchlorate (TBAP) as the supporting electrolyte (Fig. 2(b), Fig. S8, ESI†). The Ph-tpy complexes **1** and **2,** lacking any ferrocenyl moiety, displayed poor voltammetric responses giving anodic peaks (E_{pa}) near -0.26V vs. SCE without any cathodic counterpart. The corresponding peaks for complexes **3** and **4** were observed near -0.30V. The ferrocenyl moiety in complexes **3** and **4** is redox active and showed a quasi-reversible cyclic voltammetric response near +0.61V vs. SCE. This higher reduction potential value for the Fc^+/Fc couple compared to the free ferrocene (+0.42 V vs. SCE) indicates better redox stability of the ferrocene appended complexes **3** and **4**. A significantly higher positive shift (~ +0.2 V) of reduction potential compared to the free ferrocene suggests stabilization of the Fc moiety toward oxidation in the presence of the electron withdrawing terpyridyl (tpy) moiety.[29b]

[Space for Fig. 2]

X-ray crystallography

Complex **1** was structurally characterized by single crystal X-ray diffraction method (Fig. 3(a), Table 2). It crystallized in the triclinic space group $P\bar{1}$ with two molecules in the unit cell. The complex is a discrete mononuclear species with NdN_3O_6 core formed by the tridentate *N,N,N*-donor Ph-tpy and bidentate *O,O*-donor acac ligands in a nine coordinate environment. The pyridine rings of the Ph-tpy ligand lie in a planar conformation and the bidentate nitrate anions are disposed *trans* to one another. The ORTEP view of the complex is shown in Fig. 3(a) and the unit cell packing diagram is provided as supplementary material (Fig. S9, ESI†). The phenyl ring of the ph-tpy ligand makes a dihedral angle of 25.66° with the central pyridine ring of the terpyridine moiety due to steric encumbrance imposed by the hydrogen atoms (Fig. S10, ESI†). The Nd-O bond distances involving the nitrate ligands are longer than those involving the curc ligand thereby making the nitrate ligand labile in the solution phase. This lability of the nitrate ligand is reflected in ESI-MS spectra of the complexes in aqueous methanol showing a prominent peak corresponding to the $[M–(NO_3^-)]^+$ species. The Nd-O and Nd-N distances are in the range 2.3391(18)-2.566(2) Å and 2.578(2)-2.635(2) Å, respectively. Selected crystallography parameters are given in Table 2 and the bond lengths and bond angles have been enlisted in Table 3. The structural properties observed in the complexes are similar to those previously reported for analogous lanthanide complexes.[18b,56] Selected crystallography parameters are given in Table 2 and chemically significant bond lengths and bond angles have been enlisted in Table S3 (ESI†).

[Space for Fig. 3]

Theoretical studies

DFT calculations were carried out to obtain the optimized geometries and insights into the excited state properties of the Nd(III) complexes. The initial coordinates were obtained from the crystal structure of complex **1** and used for optimization. The frontier orbital calculations revealed that the HOMO of complex **4** is localized on the curcumin ligand and the LUMO is mainly confined to the Nd(III) centre (Fig. 3(b), Figs. S11–S14, Tables S2-S5, ESI†). This observation suggests that the curcumin ligand could act as an efficient photosensitizer and photo-excitation of the complex could result in electronic transitions from the HOMO centred on the curcumin moiety to the LUMO centered on Nd(III). This observation could also explain the remarkable photocytotoxicity of complex **4** in visible light. In the case of complex **2**, the HOMO is not predominantly curcumin-centred but rather derived both from the curcumin and the Nd(III) centre, while its LUMO has contributions from the tpy moiety. Consequently, the electronic excitation in complex **2** is not as facile as in complex **4** which could also explain the lower

photocytotoxicity of the former complex. In the absence of a photosensitizing curcumin moiety in complexes **1** and **3**, facile electronic transition is unlikely and hence these two control compounds are not appreciably photocytotoxic in visible light.[44]

Solubility and stability

The synthesized complexes were found to be soluble in DMF and DMSO (dimethylsulphoxide). They were moderately soluble in acetone, acetonitrile, methanol, tetrahydrofuran and chloroform but insoluble in hydrocarbon solvents. The stability of a complex in aqueous buffer is an important aspect for its application as drug and so the stability of the complexes was studied by absorption spectroscopy. The complexes were found to be stable in 10% DMEM (Dulbecco's Modified Eagle's Medium) as evidenced from the absorption study on complex **4** showing no noticeable spectral change even after 48 hours. In contrast, the free curcumin ligand was found to undergo hydrolytic degradation under identical experimental conditions (Fig. S15, ESI†). This observation indicates that the binding of curcumin to Nd(III) ion arrests its hydrolytic degradation. This finding is also supported by earlier reports on metal complexes of curcumin.[19,43-45] As mentioned earlier, the hydrolytic instability of curcumin has prevented its use as anticancer drug in clinical settings. Thus, a metal-bound formulation of curcumin could be therapeutically more effective than curcumin alone.

Cellular incorporation assay

This assay was performed to examine the cellular permeability and uptake and to optimize the incubation time of the complexes for *in-vitro* cellular assays before photo-irradiation. Uptake of complex **4** by HeLa cells at 2 h and 4 h time points was studied by fluorescence-activated cell sorting (FACS) analysis in which the intra-cellular fluorescence of the complex was monitored (Fig. 4). The number of events in the upper left quadrant of the figure indicates the population of cells in which the complex was not taken up and that in upper right quadrant represents the cell population containing the complex inside. On 2 h of incubation, complex **4** showed almost 72 % cellular uptake whereas complete internalization of the complex was observed within 4 h of incubation. Thus, we incubated the cells with the complex for 4 h for other cellular studies.

[Space for Fig. 4]

Cellular uptake and localization study

The green curcumin-derived emission from complex **4** was utilized to study the cellular localization and uptake in HeLa cells using fluorescence microscopy (Fig. 5). Complex **4** was found to accumulate significantly within 2 h of incubation which increased substantially during 4 h suggesting its accretion inside the cells. Dual staining experiment with the nucleus staining dye Hoechst 33342 (blue emission) showed primarily cytosolic localization of complex **4** within the cells as revealed from the merged images (panel (c) of Fig. 5).

[Space for Fig. 5]

Mitochondrial selectivity

Having confirmed the accumulation of complex **4** in the cytoplasm, we delved further to probe its selectivity of localization to specific cellular organelle. For this specific purpose, we examined the specificity of localization of the complex in the mitochondria (panels (d), (e), (f), Fig. 5). Dual staining of complex 4 with the mitochondria staining dye Mitotracker red showed that complex **4** specifically localized in the mitochondria of HeLa cells as evidenced from the merged image (panel (h), Fig. 5). The selective localization of complex **4** in mitochondria is indeed a significant result considering the vital role of mitochondria in mediating the intrinsic pathway of apoptosis.[44-49] There is currently substantial interests in mitochondria targeting cytotoxic drugs for applications in the chemotherapy of cancer.[46-49]

Photocytotoxicity

Having confirmed that the complexes are taken up by the cancer cells, we were interested to evaluate their cytotoxicity in the presence of visible light (400-700 nm). The *in-vitro* photodynamic efficacy and hence the photo-induced anticancer activity of a compound can be reliably assessed by measuring its cytotoxicity in terms of its IC_{50} value against cancer cells by employing the well known MTT (3-(4,5-dimethylthiazol-2-yl)-2,5-diphenyltetrazolium bromide) assay in the presence of light. Thus, the photoactivated anticancer activity of the complexes was studied by MTT assay in two human cancer cell lines, viz., human cervical carcinoma (HeLa) and estrogen receptor positive (ER+) human breast adenocarcinoma (MCF-7) in the presence of visible light (Table 3, Figs. S16–S19, ESI†). The ferrocenyl appended complex **4**, having curcumin as the photoactive ligand moiety, was found to remarkably photocytotoxic to both the cells giving IC_{50} values of 0.7±0.2 μM in HeLa and 2.1±0.6 μM in MCF-7 cells when irradiated with visible light (400–700 nm, 10 J cm^{-2}). The complex was non-toxic to both the cells in the absence of light (IC_{50} > 50 μM). On the other hand, phenyl analogue of complex **4**, viz., complex **2**, was found to be significantly less photocytotoxic to both the cells giving IC_{50} values of 4.2±0.8 μM in HeLa and 9.6±1.2 μM in MCF-7 cells while being non-toxic to both the cells in the absence of light (IC_{50} > 50 μM). Thus, a 6-fold increase in photocytotoxicity against HeLa cells and a 5-fold increase against MCF-7 cells were observed when the phenyl group in complex **2** was replaced by a ferrocenyl group in complex **4**. The control complex **1** with Ph-tpy and acac as ligands, but lacking ferrocenyl as well as photoactive curcumin moiety was not cytotoxic to both the cell lines neither in the presence nor in the absence of light (Table 3). Complex **3**, with an appended ferrocenyl moiety and acac ligand, but lacking any curcumin moiety gave IC_{50} values of 13.2±1.6 μM in HeLa and 19.9±1.8 μM in MCF-7 cells, while being non-toxic in dark. The observed photocytotoxicity of complex **3** could be due to the presence of ferrocenyl moiety. The curcumin ligand alone is known to give an IC_{50} value of 8.2±0.2 μM in visible light and 85.4±0.6 μM in dark in HeLa cells.[41a] The corresponding values in MCF-7 cells are 19.9 ± 1.4 μM in visible light and 90.3±4.9 μM in dark under similar experimental conditions.[41a] Hence, the remarkable photocytotoxicity but insignificant dark toxicity of complex **4** is unprecedented in the chemistry of lanthanide based

PDT agents. The presence of the lipophilic ferrcenyl moiety in complex **4** is likely to be responsible for the enhanced cellular uptake and photocytotoxicity of complex **4** when compared to complex **2**. Earlier, lanthanide complexes of Ph-tpy and curcumin, lacking a ferroceny moiety, were reported to show photocytotoxicty against HeLa cells in visible light.[19] Thus, we have achieved enhancement in photocytotoxicity of complex **4** by appending a ferrocenyl unit in the complex. The photocytoxic activity shown by complex **4** against the ER(+) MCF-7 cells is indeed striking since the ferrocene conjugates are known to show promising anticancer activity in both hormone dependent and independent cases.[29-31] Although, oxovanadium(IV), Fe(III), Co(III) and Cu(II) complexes of curcumin are known to show photocytotoxicity in visible light, the corresponding lanthanide(III) complexes are virtually unknown in the literature.[41-45] Selectivity of an anticancer drug in cancer cells over normal cells is an important aspect for its sucessful therapeutic application. Therefore, we studied the cytotoxicity of the most photoactive complex **4** in breast epithelial MCF-10A normal cells by the MTT assay.The results showed that complex **4** was significantly less toxic to MCF-10A cells with an IC_{50} value of 34.1±1.8 μM in light and IC_{50} > 50 μM in dark (Fig. S20, ESI†). Thus, a distinct selectivity of complex **4** for cancer cells in comparison to the normal cells was observed. This differential activity exhibited by complex **4** could be attributed to its preferential internalization into cancer cells compared to the normal cells since the cancer cells are metabolically more active than the normal cells.[44]

DCFDA assay

Reactive oxygen species (ROS) playes important role in causing apoptosis by transition metal complexes.[57,58] 2',7'-dichlorofluoresceindiacetate (DCFDA) assay is based on fluorescence assisted cell sorting (FACS) analysis that detects the formation of any intracellular ROS (Fig. 6). DCFDA is cell-permeable and upon its passive diffusion into the cells, it is retained in the intracellular level after being cleaved by the intracellular esterase enzymes. Upon oxidation by the ROS, the non-fluorescent DCFDA is converted to the highly fluorescent 2',7'-dichlorofluorescein (DCF) thereby providing an emission band centered at 529 nm. Measurements were carried out for the fluorescence of the HeLa cells alone, cells treated with only DCFDA and cells with DCFDA and complex **4** after 1 h irradiation with visible light of 400-700 nm or in dark (as controls). A large shift in the fluorescence bands was observed for the cells treated with photo-irradiated complex as compared to the cells treated with the dye alone or the dark controls. This observation suggests that the ROS are generated by the complex only on exposure to visible light but not in the dark and these species could lead to the induction of cellular apoptosis via ROS mediated cell stress.

[Space for Fig. 6]

Annexin-V-FITC/PI assay

Annexin-V-FITC is a fluorescence probe that binds phosphatidylserine in the presence of calcium(II) ion. In the early apoptotic stage, cells undergo significant morphological changes including the loss of phospholipid asymmetry. The phosphatidylserine in healthy cells remains in the interior surface of the lipid bilayer which is transferred to the outside portion of the membrane at the onset of apoptosis. This change in the membrane morphology can be detected and studies by a fluorophore conjugated annexin-V protein which is known to bind phosphatidylserine. The assay is based on dual staining of cells by annexin V-FITC (fluorescein isothiocyanate) and the DNA binding dye propidium iodide (PI). Cells undergoing early apoptosis are identified as single positive population for FITC, while necrotic cell population is stained only by PI. The double positive population represents cells in late apoptotic stage with compromised cell membrane. To find out whether the present complexes are able to trigger any apoptotic cell death in the presence of visible light, we carried out annexin-V-FITC/ PI assay using HeLa cancer cells treated with complex 4 (Fig. 7). The results were analyzed by FACS analysis. PI emits in the red region, while the annexin V-FITC dye shows green fluorescence. This assay gave an estimate of the apoptotic cells in different stages. The cells were treated with complex **4** (2 μM) followed by 1 h irradiation with visible light (400-700 nm) and the assay was performed 18 h post photo-irradiation. About 21% populations of the cells were in an early apoptotic stage and ~40% of the cells were in a late apoptotic stage. Cells population in the necrotic mode was found to be negligible. In the dark, the complex did not induce any significant cell death at this concentration. The data suggest an overall apoptotic mechanism of cell death photo-induced by the complex.

[Space for Fig. 7]

DNA binding studies

DNA is a prime target of most anticancer drugs and so we studied the binding propensity of the complexes towards calf thymus (ct) DNA by using absorption spectroscopy (Fig. 8, Table 1). The equilibrium DNA binding constant (K_b) values were in the range of 10^4-10^5 M^{-1}. The curcumin complexes **2** and **4** were found to show stronger binding affinity and hence higher K_b values than their acac analogues viz, **1** and **3**. The binding affinity of the Ph-tpy and Fc-tpy complexes was comparable indicating that the curcumin moiety in both the complexes could be responsible for interaction with the DNA. The fitting parameter (*s*) in the McGhee-von Hippel (MvH) equation gives an estimate of the number of DNA bases interacting with the complex and a value of <1.0 is typically attributed to the aggregation of hydrophobic molecules on the surface of DNA.[59] The greater value of *s* for the curcumin complexes **2** and **4** than the acac analogues **1** and **3** also suggests better DNA binding propensity of the curcumin complexes than the ph-tpy analogues.[60]

[Space for Fig. 8]

DNA thermal denaturation studies were conducted to gain information on the binding of the complexes **1–4** to ct-DNA (Fig. 9(a), Table 1). A slightly positive shift in the DNA melting temperature (ΔT_m) was observed on addition of the complex to the DNA. This increase in the DNA melting temperature suggests stabilization of the double helix on addition of the complex. The ΔT_m values of ~2.7 °C for the curcumin complexes **2** and **4** suggest their groove binding nature.[61] To delve deeper, solution viscosity measurements were carried out to examine the effect of

the added complex on the relative specific viscosity of the solution containing the ct-DNA (Fig. 9(b)). The relative specific viscosity η/η_0 (where η and η_0 are the respective specific viscosities of a DNA solution in the presence and absence of the complex) of a DNA solution is a measure of the increase in contour length of DNA as a result of the separation of base pairs caused by intercalation. Classical intercalator such as ethidium bromide (EB) causes significant increase in the viscosity of the DNA solution. A partial and/or non-intercalative DNA binder could result in less pronounced effect on the solution viscosity.[62] The groove binder Hoechst 33258 was used as a reference compound. It did not show any appreciable change in the solution viscosity of DNA. The viscosity changes observed for the complexes are suggestive of a two-step binding process in which the complex first interacts with the DNA surface followed by groove binding.[63]

[Space for Fig. 9]

DNA photocleavage studies

The DNA photocleavage activity triggered by complexes **1**–**4** was investigated using supercoiled (SC) pUC19 DNA (30 μM, 0.2 μg) in Tris-HCl/NaCl (50 mM, pH = 7.2) buffer by irradiating the samples with visible light of 454 nm (Fig. 10). The ph-tpy complexes of acac ligand, viz., **1** and **3** showed only mild DNA cleavage activity (lanes 5 and 7, Fig. 10). The curcumin complexes **2** and **4** with their photosensitizing ability showed efficient photocleavage (76% NC for **2** and 85% NC for **4**) of SC DNA at 10 μM concentration for an exposure time of 2 h (lanes 6 and 8, Fig. 10). Control experiments with only DNA, metal salts, Ph-tpy or Fc-tpy ligands did not show any apparent photocleavage of DNA (Table S6, ESI†). The complexes were not cleavage active in dark thereby excluding the possibility of any hydrolytic DNA damage (lane 4 in Fig.10). The curcumin ligand alone showed ~23% cleavage in dark. This activity could be due to generation of reactive oxygen species by curcumin in aqueous medium.[39a] However, when photo-irradiated, it showed ~43% photocleavage of DNA under similar conditions forming reactive oxygen species (ROS).[39a,19] Thus, there is substantial enhancement of DNA photocleavage activity of curcumin possibly due to its hydrolytic stabilization and efficient intersystem crossing (ISC) on complexation to the heavy Nd(III) centre.[64] Since the complexes were found to be DNA minor groove binders, their groove binding nature was examined using the well known minor groove binder distamycin-A.[65] Distamycin-A alone showed ~10% cleavage of the SC DNA in visible light. Addition of complex **2** or **4** to the distamycin-A bound DNA showed significant inhibition of photocleavage activity thereby suggesting the minor groove binding preference of the complexes (lanes 9 and 10 in Fig. 10).[66]

[Space for Fig. 10]

Mechanistic aspects of DNA photocleavage

To obtain mechanistic insights, we carried out DNA photocleavage studies using the ferrocene appended curcumin complex **4** in the presence of different additives (Fig. 11, Figs. S21, S22, ESI†). The DNA cleavage reactions involving molecular oxygen could occur by different two pathways, namely, the type-II process that produces singlet oxygen ($^1O_2$) or a photo-redox process that produces hydroxyl radical ($^\bullet OH$).[67] Addition of singlet oxygen quenchers such as sodium azide, 2,2,6,6-tetramethyl-4-piperidone (TEMP) or 4-diazabicyclo[2.2.2]octan (DABCO) to DNA resulted in partial inhibition of photocleavage activity of the complex. Similarly, the addition of hydroxyl radical scavengers such as DMSO or catalase also caused partial inhibition in the DNA photocleavage activity. Addition of superoxide dismutase (SOD) did not inhibit the photcleavage activity the complexes thereby ruling out the involvent of superoxide radical. These observations suggest the involvement of both $^1O_2$ and $^\bullet OH$ as the cleavage active ROS. Furthermore, an enhancement in the photocleavage activity of the complex was seen in D_2O due to longer lifetime of $^1O_2$ in this solvent than in water.[68] Thus, the formation of $^1O_2$ could be due to the photoactive curcumin moiety via a type-II process while the formation of hydroxyl radicals could result from electron transfer from the photo-excited ligand to molecular oxygen generating a radical cation.[69]

[Space for Fig. 11]

Conclusions

In conclusion, we report here the synthesis, characterization and visible light induced cytotoxicity of a series of mixed-ligand Nd(III) complexes of functionalized terpyridine bases and curcumin. The curcumin complexes **2** and **4** are remarkably photocytotoxic to HeLa and MCF-7 cells but non-toxic in the absence of light. The ferrocenyl appended complex **4** is significantly more photocytotoxic than its phenyl analogue-complex **2**, although both possess curcumin as the photosensitizer ligand. The control complexes **1** and **3** having the acac ligand but lacking any curcumin moiety were neither active in light nor in the dark. Thus, the presence of the ferrocenyl unit in complex **4** could result in significant enhancement in cellular uptake and photocytotoxicity of complex **4**. Complex **4** accumulates within the mitochondria of HeLa cells and induces apoptosis which is triggered by the visible light-induced formation of ROS. The complexes, particularly **2** and **4**, are moderately strong binders but potent cleavers of plasmid DNA. Thus, complex **4** holds significant chemotherapeutic potential and warrants further work to design and develop ferrocene appended lanthanide-curcumin complexes with better tumour selectivity and enhanced photocytotoxicity for potential photochemotherapeutic applications. Further experimental efforts are in progress in our laboratory to develop such complexes for potential applications in the PDT of cancer.

Experimental

Materials

Unless otherwise mentioned, all the reagents and chemicals used in the present work were obtained from commercial suppliers and used as received. Solvents were purified prior to their use by following standard literature methods.[70] Curcumin (95% curcuminoid content, *ca* 80% curcumin content) was obtained from Sigma-Aldrich, U.S.A. and separated into their individual components by following a literature procedure.[71] Tris-(hydroxymethyl)aminomethane-HCl (Tris-HCl) buffer solution

(pH = 7.2) was prepared using deionized and sonicated double distilled water. Dulbecco's Modified Eagle's medium (DMEM), propidium iodide, Hoechst 33342, 3-(4,5-dimethylthiazol-2-yl)-2,5-diphenyltetrazolium bromide (MTT) and 2',7'-dichlorofluorescein diacetate (DCFDA), calf thymus (ct) DNA, agarose (molecular biology grade), distamycin-A, catalase, 2,2,6,6-tetramethyl-4-piperidone (TEMP), 1,4-diazabicyclo[2.2.2]octan (DABCO) and ethidium bromide (EB) were procured from Sigma-Aldrich (U.S.A) and used as received. Mito-Tracker Red was procured from Invitrogen, U.S.A. Supercoiled (SC) pUC19 DNA (cesium chloride purified) was purchased from Bangalore Genie (India) The terpyridine derivatives, viz., 4′-phenyl-2,2′:6′,2″-terpyridine (Ph-tpy) and 4′-ferrocenyl-2,2′:6′,2″-terpyridine (Fc-tpy) were prepared by following literature procedures.[72]

Measurements

The elemental analyses were carried out on a Thermo Finnigan Flash EA 1112 CHNS analyzer. The infrared (IR) spectra of pure solid samples were recorded on a Bruker ATR FT-IR spectrometer. The UV-Visible absorption spectra were recorded on a Perkin Elmer Lambda 650 spectrophotometer. The molar conductivity measurements were done using a properly calibrated digital conductivity meter (Labtronics, India). Room temperature electrochemical measurements were carried out on a Biologic SP-50 Potentiostat/Galvenostat (Biologic Instruments, France) with a three electrode setup consisting of a platinum working electrode, platinum wire auxiliary electrode, and calomel reference electrode (SCE) at a scan rate of 100 mVs^{-1}. The electrochemical measurements were made using solutions of the metal complexes prepared in HPLC grade DMF. Tetrabutylammonium perchlorate (TBAP, 0.1M) was used as a supporting electrolyte in DMF. The electrospray ionization mass spectra (ESI-MS) were recorded using Agilent Technologies 6538 UHD Accurate-mass Q-TOF LC/MS mass spectrometer. The fluorescence quantum yields were determined using a PerkinElmer LS 55 fluorescence spectrometer using coumarin-153 laser dye as a reference with a known quantum yield (Φ) value of 0.56 in acetonitrile.[73] The samples for quantum yield measurements were deoxygenated prior to experiments. The sample and the reference were excited at 430 nm, maintaining nearly equal absorbance. The integrated emission intensity was calculated using Origin Pro 8.1 software and the quantum yield was calculated using the equation $\Phi_S/\Phi_R = (A_S/A_R) \times [(OD)_R/(OD)_S] \times [(n_S)^2/(n_R)^2]$, where, Φ_S and Φ_R are the fluorescence quantum yields of the sample and reference respectively, A_S and A_R are the area under the fluorescence spectra of the sample and the reference respectively, $(OD)_S$ and $(OD)_R$ are the respective optical densities of the sample and the reference solution at the wavelength of excitation, and n_S and n_R are the respective refractive indices of the solvents used for the sample and the reference.[74,75] The fluorescence microscopic investigations were carried out using ApoTome.2 fluorescence microscope. The flow cytometric analysis was performed using FACS Calibur (Becton Dickinson (BD) cell analyzer) at FL1 channel (595 nm).

Syntheses of the complexes 1–4

The complexes were prepared by a general two-step synthetic route. An ethanol solution (15 ml) of $Nd(NO_3)_3.6H_2O$ (0.44 g, 1.0 mmol) was added dropwise to a dichloromethane solution (15 ml) of the terpyridine ligand (Ph-tpy, 0.31 g; Fc-tpy, 0.35 g; 1.0 mmol) under nitrogen atmosphere. The resulting reaction mixture was stirred for 1 hour at room temperature and subsequently cooled to 0°C to obtain crystalline solids of $[Nd(Ph\text{-}tpy)(NO_3)_3]$ or $[Nd(Fc\text{-}tpy)(NO_3)_3]$ as the precursor complex. The complex was filtered, washed with ice-cold ethanol followed by diethyl ether and finally dried in vacuum and used directly in the next step without further treatment.

To a deaerated methanol/acetonitrile suspension (1:1 v/v, 20 ml) of the precursor complex $[Nd(Ph\text{-}tpy)(NO_3)_3]$ (0.32 g, 0.5 mmol) or $[Nd(Fc\text{-}tpy)(NO_3)_3]$ (0.34 g, 0.5 mmol) was added a deaerated methanol solution (10 ml) of the *β*-diketone ligand (0.05 g, Hacac; 0.18 g, Hcurc, 0.5 mmol) previously neutralized with triethylamine (0.07 ml, 0.5 mmol). After stirring for 1 h at room temperature, a clear solution was obtained in the case of complexes **1** and **3** while complexes **2** and **4** precipitated as brick red solids. Slow evaporation of the solution of complex **1** afforded single crystals suitable for diffraction studies while complex **3** appeared as microcrystalline solid. The solids were isolated, washed with cold methanol followed by diethyl ether and finally dried in vacuum over P_4O_{10}. The characterization data for the complexes are given below.

$[Nd(Ph\text{-}tpy)(acac)(NO_3)_2]$ (1): Yield: ~81%. Anal. Calcd. for $C_{26}H_{22}N_5O_8Nd$: C, 46.15; H, 3.28; N, 10.35; Found: C, 46.35; H, 3.36; N, 10.43. ESI–MS in 5% aqueous methanol: *m/z* 614.09 $[M–(NO_3^-)]^+$. FT–IR data/ cm^{-1}: 1590 s, 1531 s, 1498 vs, 1410 s, 1383 s, 1286 s,1175 m, 1012 s, 922 w, 794 w, 760 s, 735 m, 697 m, 638 m (vs, very strong; s, strong; m, medium; w, weak; sbr, strong broad). UV–visible in 5% aqueous DMF [λ_{max}/nm (ε/ M^{-1} cm^{-1})]: 280 (71,200). Molar conductivity in DMF at 298 K [Λ_M / S cm^2 mol^{-1}]: 85.

$[Nd(Ph\text{-}tpy)(curc)(NO_3)_2]$ (2): Yield: ~78%. Anal. Calcd. for $C_{42}H_{34}N_5O_{12}Nd$: C, 53.38; H, 3.63; N, 7.41. Found: C, 53.51; H, 3.51; N, 7.46. ESI–MS in 5% aqueous methanol: *m/z* 880.11 $[M–(NO_3^-)]^+$. FT–IR data/ cm^{-1}: 3390 br, 1592 s, 1495 vs, 1390 s, 1286 s, 1216 m, 1154 m, 1120 s, 1025 w, 967 m, 820 w, 760 w. UV–visible in 5% aqueous DMF [λ_{max}/nm (ε/ M^{-1} cm^{-1})]: 276 (60,600), 430 (54,300), 455 (48,500) . Molar conductivity in DMF at 298 K [Λ_M / S cm^2 mol^{-1}]: 71.

$[Nd(Fc\text{-}tpy)(acac)(NO_3)_2]$ (3): Yield: ~78%. Anal. Calcd. for $C_{30}H_{26}N_5O_8FeNd$: C, 45.92; H, 3.34; N, 7.12; Found: C, 46.06; H, 3.38; N, 7.02. ESI–MS in 5% aqueous methanol: *m/z* 722.08 $[M–(NO_3^-)]^+$. FT–IR data/ cm^{-1}: 1596 s, 1540 m, 1505 s, 1454 vs, 1420 s, 1380 vs, 1302 m, 1273 m, 1254 m, 1160 w, 1007 s, 930 w, 826 w, 788 s, 760 w, 731 m, 655 w. UV–visible in 5% aqueous DMF [λ_{max}/nm (ε/ M^{-1} cm^{-1})]: 287 (57,200), 365 sh (2,800), 465 (1,457). Molar conductivity in DMF at 298 K [Λ_M / S cm^2 mol^{-1}]: 82.

$[Nd(Fc\text{-}tpy)(curc)(NO_3)_2]$ (4): Yield:~76%. Anal. Calcd. for $C_{46}H_{38}N_5O_{12}FeNd$: C, 52.47; H, 3.64; N, 5.30. Found: C, 52.60; H, 3.52; N, 5.35. ESI–MS in 5% aqueous methanol: *m/z* 990.14 $[M–(NO_3^-)]^+$. FT–IR data/ cm^{-1}: 3385 sbr, 1602 s, 1502 s, 1423 s, 1388 vs, 1276 vs, 1153 s, 1118 m, 1034 m, 1001 s, 970 m, 816 m, 786 m, 731 w, 668 w, 633 w. UV–visible in 5% aqueous DMF

[λ_{max}/nm (ε/ M^{-1} cm^{-1})]: 279 (68,000), 430 (63,000), 455 (56,100). Molar conductivity in DMF at 298 K [Λ_M / S cm^2 mol^{-1}]: 69.

X-ray crystallographic procedures

The crystal structure of **1** was obtained by the single crystal X-ray diffraction technique. Single crystals of **1** were grown by slow evaporation of a solution of the complex in methanol. Crystal mounting was done on glass fiber with epoxy cement. All geometric and intensity data were collected at room temperature using an automated Bruker SMART APEX CCD diffractometer equipped with a fine focus 1.75 kW sealed tube Mo-K_α X-ray source (λ = 0.71073 Å) with increasing ω (width of 0.3° per frame) at a scan speed of 4 seconds per frame. Intensity data, collected using ω-2θ scan mode, were corrected for Lorentz–polarization effects and for absorption.[76] Patterson and Fourier techniques were used to solve the structures and refinement was done by full matrix least squares method using SHELX system of programs.[77] The hydrogen atoms belonging to the complexes were in their calculated positions and refined using a riding model. All non-hydrogen atoms were refined anisotropically. The perspective views of the molecules were obtained by ORTEP.[78] The CCDC number assigned to complex **1** is 1425834.

Computational methodology

To rationalize the photophysical properties and to obtain a better understanding of the molecular structure and electronic nature of the complexes, DFT computational studies were performed using B3LYP hybrid functional and LANL2DZ (pseudo-potential) basis-set for Fe, MWB28 (pseudo-potential) basis set for Nd and 3-21G basis set for other types of atoms, using quadratic convergence criteria, as incorporated in *Gaussian* 09 software package.[79,80] In order to ascertain stationary points, frequency tests were performed after optimisation of the ground-state structures.

Cell culture

HeLa (human cervical carcinoma), MCF-7 (human breast adenocarcinoma) and MCF-10A (human breast epithelial cell) cells were maintained in DMEM supplemented with 10% FBS, 100 IU mL^{-1} of penicillin, 100 µg mL^{-1} of streptomycin and 2 mM of Glutamax at 37 °C in a humidified incubator at 5% CO_2. The adherent cultures were grown as monolayer and were passaged once in 4-5 days by trypsinizing with 0.25% Trypsin-EDTA.

Cellular incorporation assay

For flow cytometric analysis, ~0.3x10^6 HeLa cells were plated per well of a 6-well tissue culture plate in Dulbecco's Modified Eagle Medium (DMEM) containing 10% FBS. After 24 h of incubation at 37 °C in a CO_2 incubator, complex **4** (1 µM) was added to the cells at 2 and 4 h incubation time intervals in the dark, cells were trypsinized, transferred into 1.5 ml centrifuge tubes, washed once with chilled PBS and fixed by adding 800 µl of chilled 70% ethanol drop-wise with constant and gentle vortexing to prevent cell aggregation. The cell suspension was incubated at -20 °C for 6 h. The fixed cells were then washed twice with 1.0 ml of chilled PBS by centrifuging at 4000 rpm for 5 min at 4° C. The supernatant was discarded and the cell pellet was suspended in 200 µl of PBS containing 10 µg ml^{-1} of DNAse-free RNAse for 12 h at 37° C for digesting the cellular RNA. After RNAse digestion, cells were washed twice with DPBS and the analysis was performed using FACS Calibur (Becton Dickinson (BD) cell analyzer) at FL2 channel.

Fluorescence microscopy experiments

HeLa cells (~4 x 10^4 cells/mm^2), plated on cover slips, were incubated with complex **4** (30 µM) for 2 h and 4 h in the dark, fixed with 4% paraformaldehyde for 10 min at room temperature (RT) and washed with PBS. This was followed by staining with Hoechst 33342 dye for 10 min at 25 °C. The cells were washed, mounted in 90% glycerol solution containing Mowiol, an anti-fade reagent, and sealed. Images were acquired using Apotome.2 fluorescence microscope (Carl Zeiss, Germany) using an oil immersion lens at 63 X magnification. The images were analyzed using the AxioVision Rel 4.8.2 (Carl Zeiss, Germany) software.[81] For sub-cellular localization study, HeLa (~4 x 10^4 cells/mm^2) were incubated with 30 µM of complex **4** for 4 h in the dark, following which, the cells were treated with 500 nM of mitotracker red (MTR) in serum-free medium for 30 min at 37 ºC. The cells were then washed with PBS, mounted on slides and sealed with nail-paint. The images were acquired using Apotome.2 fluorescence microscope at 63X magnification and analysed using AxioVision Rel 4.8.2.

Cytotoxicity

The cytotoxicity of the complexes was studied using MTT assay in light and dark conditions in human cervical carcinoma (HeLa) and human breast adenocarcinoma (MCF-7) cells following reported procedures.[82] The MTT assay method is based on the ability of mitochondrial dehydrogenases of viable cells to cleave the tetrazolium rings of MTT, forming dark purple membrane impermeable crystals of formazan that can be estimated from the spectral measurements in DMSO at 540 nm.[46] Photo-irradiation was done with a broad band visible light (400−700 nm, 10 J cm^{-2}) using Luzchem Photoreactor (Model LZC-1, Ontario, Canada, Sylvania fluorescent white tubes with a fluence rate of 2.4 mW cm^{-2} to provide a total dose of 10 J cm^{-2}). The absorbance was measured at 540 nm using a Molecular Devices Spectra Max M5 plate reader. Cytotoxicity of the complexes was measured as the percentage ratio of the absorbance of the treated cells to the untreated controls. The cytotoxicity was expressed in terms of the IC_{50} values which were determined by nonlinear regression analysis using Graph Pad Prism 5.

DCFDA assay for ROS generation

DCFDA assay was carried out to detect any generation of intracellular ROS.[83] Cell permeable DCFDA on oxidation by cellular ROS generates green fluorescent 2′,7′-dichlorofluorescein (DCF) with an emission maxima around 525 nm.[84] To detect intracellular ROS generation, HeLa cells were incubated with 2 µM of complex **4** for 4 h followed by photo-exposure to visible light (400-700 nm) for 1 h in PBS (50 mM phosphate buffer, pH, 7.2 containing 150 mM NaCl). After harvesting the cells by trypsinization, a single cell suspension of 1x10^6 cells ml^{-1} was

prepared. The cells were then treated with 10 μM DCFDA in dark for 15 min at room temperature. The distribution of the HeLa cells, stained by DCFDA, was determined by FACS analysis.

Annexin-V FITC and propidium iodide (PI) assay

To investigate the pathway of cell death, HeLa cells (4 x 10^5 cells ml^{-1}) were incubated with complex **4** (2 μM) in 10% DMEM for 4 h, followed by irradiation with visible light of 400-700 nm for 1 h. The cells were then cultured for 18 h, harvested and washed with chilled PBS at 4°C. The cells were then re-suspended in 100 μl Annexin-V binding buffer (100 mM HEPES/ NaOH, pH 7.4 containing 140 mM NaCl and 2.5 mM $CaCl_2$), stained with Annexin-V FITC and PI, and incubated for 15 min in dark. A 400 μl of binding buffer was added to the cells after incubation, and flow cytometry was done foranalysis.[85]

DNA binding experiments

DNA binding experiments were carried in Tris-HCl/NaCl buffer (5 mM Tris-HCl, 5 mM NaCl, pH 7.2) using DMF solution of the complexes **1**-**4**. Calf thymus (ct) DNA (*ca*. 350 μM NP) in gave a ratio of UV absorbances at 260 and 280 nm of 1.9:1 indicating that the DNA sample was apparently free from proteins. The concentration of ct DNA was estimated from its absorbance at 260 nm having a known extinction coefficient value (ε) of 6600 M^{-1} cm^{-1}.[86] Absorption titration measurements were done by varying the concentration of the ct DNA but maintaining a constant concentration of the metal complex. Due corrections were applied to the absorbance of ct DNA itself. Each spectrum was recorded after incubation of the sample for 5 minutes. The equilibrium binding constant (K_b) and the binding site size (s) of the complexes **1**–**4** were calculated by the McGhee-von Hippel (MvH) method. The expression given Bard *et al.* was used and the change of the absorbances of the spectral bands with increasing concentration of ct DNA was monitored. The non-linear regression analysis was done by using equation $(\varepsilon_a - \varepsilon_f)/(\varepsilon_b - \varepsilon_f) = (b - (b^2 - 2K_b^2C_t[DNA]_t/s)^{1/2})/2K_bC_t$, where $b = 1 + K_bC_t + K_b[DNA]_t/2s$ and ε_a is the extinction coefficient observed for the absorption band at a given DNA concentration, ε_f is the extinction coefficient of the complex free in solution, ε_b is the extinction coefficient of the complex when fully bound to DNA, K_b is the equilibrium binding constant, C_t is the total metal complex concentration, $[DNA]_t$ is the DNA concentration in nucleotides and s is the binding site size in base pairs.[59,87] The non-linear least-squares analyses were carried out using Origin Lab 8.0 software.

DNA thermal denaturation (melting) experiments were done by monitoring the absorbance of ct DNA (200 μM) at 260 nm at various temperatures, both in the absence and presence of the complexes (20 μM). Measurements were carried out using a Perkin Elmer Lambda 650 spectrophotometer with a Peltier PTP-1+1 temperature controller at an increase rate of 0.5 °C/min of the solution. Viscometric measurements were carried out with a vibration-free Mansingh Survismeter (Borosil, Singapore Govt. Patent No. 12609) that was thermostated at 37 ºC in a constant temperature water bath. The concentration of ct DNA was 150 μM in NP (nucleotide pair) and the flow times were measured using an automated timer. Each sample was measured 3 times and an average flow time was calculated. Data were plotted as $(\eta/\eta_0)^{1/3}$ vs. [complex]/[DNA], where η is the viscosity of DNA in the presence of complex and η_0 is that of DNA alone. The viscosity values were calculated from the observed flow time of DNA-containing solutions (t) corrected for that of the buffer alone (t_0), $\eta = (t - t_0)/t_0$ and due corrections were made for the viscosity of DMF solvent present in the solution.

DNA cleavage experiments

The cleavage of supercoiled (SC) pUC19 DNA (30 μM, 0.2 μg, 2686 base-pairs) was studied by agarose gel electrophoresis method. The photocleavage experiments on DNA were carried out by using visible light of 454 nm with a laser source (Spectra Physics continuous-wave Ar–Kr mixed-gas ion laser, model: Stabilities 2018-RM; laser power: 60 mW). Eppendorf vials were used for photocleavage experiments in a dark room at room temperature using SC DNA (1 μL, 30 μM) in 50 mM Tris-HCl buffer (pH 7.2) containing 50 mM NaCl and the complex (2 μL) with varied concentrations. The concentration of the complex in DMF or the additives in the buffer corresponded to the quantity in 2 μL stock solution after dilution to a final volume of 20 μL using Tris-HCl buffer. After light irradiation, each sample was incubated for 1 h at 37 °C and analyzed for the photocleavage products using gel electrophoresis. Mechanistic studies were carried out using different additives (NaN_3, 0.5 mM; TEMP, 0.5 mM; DABCO, 0.5 mM; DMSO, 4 μL; KI, 0.5 mM; catalase, 4 units) prior to the addition of the complex. For experiment in D_2O, this solvent was used instead of water for dilution of the sample to a final volume of 20 μL. The samples after incubation in a dark chamber were added to the loading buffer containing 0.25% bromophenol blue, 0.25% xylene cyanol, 30% glycerol (3 μL) and the solution was finally loaded on 1% agarose gel containing 1 μg/mL ethidium bromide (EB). Electrophoresis was done in a dark room for 2 h at 50 V in TAE (Tris-acetate EDTA) buffer. Bands so separated were visualized in UV light and photographed. The extent of cleavage of SC DNA was measured from the intensities of the bands using a Gel Documentation System (UVITEC). Corrections were made for the low level of nicked circular (NC) form of DNA present in the original SC DNA sample and for the low affinity of ethidium bromide to SC compared to NC and linear forms of DNA.[88] The observed error in measuring the band intensities was in the range 2-5%.

Acknowledgements

Work in the laboratory of A.H. is funded by the Department of Biotechnology (DBT), Government of India (U-Excel grant: BT/401/NE/U-Excel/2013). S.B. thanks IISc, Bangalore for a postdoctoral fellowship. T.S. thanks the DBT for research fellowship and S. M thanks the CSIR for SPM research fellowship. We acknowledge the single crystal diffractometer facility of SAIF, Department of Instrumentation & USIC, Gauhati University. We thank Professor A. R. Chakravarty and Professor A. A. Karande for their help in this work.

References

1 A. Juarranz, P. Jaén, F. Sanz-Rodríguez, J. Cuevas and S. González, *Clin. Trans. Oncol.,* 2008, **10**, 148-154.

2 P. Agostinis, K. Berg, K. A. Cengel, T. H. Foster, A. W. Girotti, S. O. Gollnick, S. M. Hahn, M. R. Hamblin, A. Juzeniene, D. Kessel, M. Korbelik, J. Moan, P. Mroz, D. Nowis, J. Piette, B. C. Wilson and J. Golab, *Ca-Cancer J. Clin.,* 2011, **61**, 250–281.

3 (a) A. E. O'Connor, W. M. Gallagher and A. T. Byrne, *Photochem. Photobiol.*, 2009, **85**, 1053-1074; (b) H. J. Nyst, I. B. Tan, F. A. Stewart and A. J. M. Balm, *Photodiag. Photodyn. Ther.,* 2009, **6**, 3-11.

4 J. Gray and G. Fullarton, *Photodiag. Photodyn. Ther.,* 2007, **4**, 151-159.

5 B. Q. Spring, I. Rizvi, N. Xua and T. Hasan, *Photochem. Photobiol. Sci.,* 2015, **14**, 1476-1491.

6 (a) R. R. Allison, R. Cuenca, G. H. Downie, M. E. Randall, V. S. Bagnato and C. H. Sibata, *Photodiag. Photodyn. Ther.,* 2005, **2**, 51-63; (b) M.-F. Zuluaga and N. Lange, *Curr. Med. Chem.,* 2008, **15**, 1655-1673.

7 (a) M. Kar and A. Basak, *Chem. Rev.,* 2007, **107**, 2861-2890; (b) J. Mao, Y. Zhang, J. Zhu, C. Zhang and Z. Guo, *Chem. Commun.,* 2009, 908-910.

8 (a) I. Kinzler, E. Haseroth, C. Hauser and A. Rűck, *Photochem. Photobiol. Sci.,* 2007, **6**, 1332-1340; (b) J. P. Celli, B. Q. Spring, I. Rizvi, C. L. Evans, K. S. Samkoe, S. Verma, B. W. Pogue and T. Hasan, *Chem. Rev.,* 2010, **110**, 2795-2838; (c) M. Chakrabarti, N. L. Banik and S. K. Ray, *Plos One,* 2013, **8**, e55652.

9 (a) "Metal Complexes for Photodynamic Therapy": R. Bonnett in *Comprehensive Coordination Chemistry*, Vol. 2 (Eds.: J. A. McCleverty, T. Meyer), Elsevier Pergamon, Oxford, 2004, p. 945; (b) N. L. Fry and P. K. Mascharak, *Acc. Chem. Res.* 2011, **44**, 289-298.

10 (a) N. J. Farrer and P. J. Sadler, *Aust. J. Chem.,* 2008, **61**, 669-674; (b) N. J. Farrer, L. Salassa and P. J. Sadler, *Dalton Trans.,* 2009, **48**, 10690-10701.

11 (a) A. Bergamo and G. Sava, *Dalton Trans.,* 2011, **40**, 7817-7823; (b) U. Schatzschneider, *Eur. J. Inorg. Chem.* **2010**, 1451-1467.

12 (a) H. T. Chifotides and K. R. Dunbar, *Acc. Chem. Res.,* 2005, **38**, 146-156; (b) A. M. Angeles-Boza, H. T. Chifotides, J. D. Aguirre, A. Chouai, P. K.-L. Fu, K. R. Dunbar and C. Turro, *J. Med. Chem.,* 2006, **49**, 6841-6847.

13 (a) S. P. Fricker, *Chem. Soc. Rev.,* 2006, **35**, 524-533; (b) T. Storr, K. H. Thompson and C. Orvig, *Chem. Soc. Rev.,* 2006, **35**, 534-544.

14 E. J. New, D. Parker, D. G. Smith and J. W. Walton, *Curr. Opin. Chem. Biol.,* 2010, **14**, 238-246.

15 (a) E. J. Werner, A. Datta, C. J. Jocher and K. N. Raymond, *Angew. Chem. Int. Ed.,* 2008, **47**, 8568-8580; (b) P. Caravan, *Acc. Chem. Res*., 2009, **42**, 851-862.

16 (a) E. J. New, A. Congreve and D. Parker, *Chem. Sci.,* 2011, **1**, 111-118; (b) J. C. G. Bünzli, *Chem. Rev.,* 2010, **110**, 2729-2755.

17 (a) A. Hussain, D. Lahiri, M. S. A. Begum, S. Saha, R. Majumdar, R. R. Dighe and A. R. Chakravarty, *Inorg. Chem.,* 2010, **49**, 4036-4045; (b) A. Hussain and A. R. Chakravarty, *J. Chem Sci.,* 2012, **124**, 1327-1342.

18 (a) A. Hussain, S. Gadadhar, T. K. Goswami, A. A. Karande and A. R. Chakravarty, *Dalton Trans.,* 2011, **41**, 885-895; (b) A. Hussain, S. Gadadhar, T. K. Goswami, A. A. Karande and A. R. Chakravarty, *Eur. J. Med. Chem*., 2012, **50**, 319-331.

19 A. Hussain, K. Somyajit, B. Banik, S. Banerjee, G. Nagaraju and A. R. Chakravarty, *Dalton Trans.,* 2013, **42**, 182-195.

20 J. L. Sessler and R. A. Miller, *Biochem. Pharmacol*., 2000, **59**, 733-739.

21 G.-J. Chen, X. Qiao, J.-L. Tian, J.-Y. Xu, W. Gu, X. Liu and S.-P. Yan, *Dalton Trans*., 2010, **39**, 10637-10643.

22 W.-H. Wei, Z. Wang, T. Mizuno, C. Cortez, L. Fu, M. Sirisawad, L. Naumovski, D. Magda and J. L. Sessler, *Dalton Trans.,* 2006, 1934-1942.

23 (a) G. Gasser, I. Ott and N. Metzler-Nolte, *J. Med. Chem*., 2011, **54**, 3-25; (b) G. Gasser and N. Metzler-Nolte, *Curr. Op. Chem. Biol.,* 2012, **16**, 84-91; (c) S. S. Braga and A. M. S. Silva, *Organometallics,* 2013, **32**, 5626−5639; (d) C. Ornelas, *New J. Chem.,* 2011, **35**, 1973–1985.

24 (a) G. S. Smith and B. Therrien, *Dalton Trans.,* 2011, **40**, 10793-10800; (b) C. G. Hartinger and P. J. Dyson, *Chem. Soc. Rev.,* 2009, **38**, 391-401; (c) C. G. Hartinger, N. Metzler-Nolte and P. J. Dyson, 2012, **31**, 5677–5685.

25 (a) A. F. A. Peacock and P. J. Sadler, *Chem. Asian J.* **2008**, *3*, 1890-1899; (b) E. Meggers, *Chem. Commun.,* 2009*,* 1001-1010.

26 M. F. R Fouda,. M. M. Abd-Elzaher, R. A. Abdelsamaia and A. A Labib, *Appl. Organometal. Chem.,* 2007, **21**, 613-625.

27 A. Nguyen, S. Top, A. Vessieres, P. Pigeon, M. Huche, E. A. Hillard and G. Jaouen, *J. Organometal. Chem.,* 2007, **692**, 1219-1225.

28 D. Dive and C. Biot, *ChemMedChem,* 2008, **3**, 383-391.

29 (a) B. Maity, M. Roy, S. Saha and A. R. Chakravarty, *Organometallics,* 2009, **28**, 1495-1505; (b) B. Maity, M. Roy, B. Banik, R. Majumdar, R. R. Dighe and A. R. Chakravarty, *Organometallics,* 2010, **29**, 3632-3641.

30 (a) B. Balaji, B. Banik, P. K. Sasmal, B. Maity, R. Majumdar, R. R. Dighe and A. R. Chakravarty, *Eur. J. Inorg. Chem.,* 2012, 126-135; (b) B. Balaji, K. Somyajit, B. Banik, G. Nagaraju and A. R. Chakravarty, *Inorg. Chim. Acta.,* 2013, **400**, 142-150.

31 T. K. Goswami, S. Gadadhar, M. Roy, M. Nethaji, A. A. Karande and A. R. Chakravarty, *Organometallics*, 2012, **31**, 3010–3021.

32 (a) B. B. Aggarwal, K. B. Harikumar, *Int. J. Biochem. Cell Biol.,* 2009, **41**, 40-59; (b) M.-H. Teiten, S. Eifes, M, Dicato, M. Diederich, *Toxins,* 2010, **2**, 128-162; (c) R. A. Sharma, W. P. Steward and A. J. Gescher, *Adv. Exp. Med. Biol.,* 2007, **595**, 453-470.

33 (a) G. Bar-Sela, R. Epelbaum, M. Schaffer, *Curr. Med. Chem.* **2010**, *17*, 190-197; (b) J. L. Ji, X. F. Huang and H. L. Zhu, *Anticancer Agents Med. Chem.,* 2012, **12**, 210-218.

34 (a) N. Dhillon, B. B. Aggarwal, R. A. Newman, R. A. Wolff, A. B. Kunnumakkara, J. L. Abbruzzese, C. S. Ng, V. Badmaev and R. Kurzrock, *Clin. Cancer Res.,* 2008, **14**, 4491-4499; (b) C. H. Hsu and A. L. Cheng, *Adv. Exp. Med. Biol.,* 2007, **595**, 471-480.

35 P. Anand, S. G. Thomas, A. B. Kunnumakkara, C. Sundaram, K. B. Harikumar, B. Sung, S. T. Tharakan, K. Misra, I. K. Priyadarsini, K. N. Rajasekharan and B. B. Aggarwal, *Biochem. Pharmacol.,* 2008, **76**, 1590-1611.

36 (a) S. Wanninger, V. Lorenz, A. Subhan and F. T. Edelmann, *Chem. Soc. Rev.,* 2015, **44**, 4986-5002; (b) S. Banerjee and A. R. Chakravarty, *Acc. Chem. Res.,* 2015, **48**, 2075–2083.

37 (a) A. K. Renfrew, N. S. Bryce and T. W. Hambley, *Chem. Sci.,* 2013, **4**, 3731- 3739; b) D. Pucci, T. Bellini, A. Crispini, I. D′. Agnano, P. F. Liguori, P. Garcia-Orduña, S. Pirillo, A. Valentini and G. Zanchetta, *Med. Chem. Commun.,* 2012**, 3**, 462-468.

38 (a) R. Pettinari, F. Marchetti, C. Pettinari, F. Condello, A. Petrini, R. Scopelliti, T. Riedel and P. J. Dyson, *Dalton Trans.,* 2015, **44**, 20523-20531; (b) M. Sagnou, D. Benaki, C. Triantis, T. Tsotakos, V. Psycharis, C. P. Raptopoulou, I. Pirmettis, M. Papadopoulos and M. Pelecanou, *Inorg. Chem.,* 2011, **50**, 1295-1303.

39 (a) I. K. Priyadarsini, *J. Photochem. Photobiol. C: Photochem. Rev.,* 2009, **10**, 81-95; (b) T. A. Dahl, P. Bilski, K. J. Reszka and C. F. Chignell, *Photochem. Photobiol.,* 1994, **59**, 290-294.

40 (a) A. Bernd, *Phytochem. Rev.,* 2014, **13**, 183-189; (b) K. Park and J.-H. Lee, *Oncol. Rep*., 2007, **17**, 537-540.

41 (a) S. Banerjee, A. Dixit, A. A. Karande and A. R. Chakravarty, *Eur. J. Inorg. Chem.,* 2015, 447-457; (b) S. Banerjee, P. Prasad, I. Khan, A. Hussain, P. Kondaiah and A. R. Chakravarty, *Z. Anorg. Allg. Chem.,* 2014*,* **640**, 1195-1204; (c) P. Prasad, I. Pant, I. Khan, P. Kondaiah and A. R. Chakravarty, *Eur. J. Inorg. Chem.,* 2014, 2420-2431.

42 (a) T. K. Goswami, S. Gadadhar, B. Gole, A. A. Karande and A. R. Chakravarty, *Eur. J. Med. Chem.,* 2013, **63**, 800-810; (b) B. Banik, K. Somyajit, G. Nagaraju and A. R. Chakravarty, *Dalton Trans.,* 2014, **43**, 13358-13369.

43 (a) S. Banerjee, P. Prasad, A. Hussain, I. Khan, P. Kondaiah and A. R. Chakravarty, *Chem. Commun.,* 2012, **48**, 7702-7704; (b) S. Banerjee, I. Pant, I. Khan, P. Prasad, A. Hussain, P. Kondaiah and A. R. Chakravarty, *Dalton Trans.,* 2015, **44**, 4108-4122.

44 T. Sarkar, S. Banerjee and A. Hussain, *RSC Adv.,* 2015, **5**, 29276–29284.

45 T. Sarkar, R. J. Butcher, S. Banerjee, S. Mukherjee and A. Hussain, *Inorg. Chim. Acta,* 2016, **439**, 8-17.

46 A. K. Renfrew, N. S. Bryce and T. Hambley, *Chem. Eur. J.*, 2015, **21**, 15224-15234.

47 (a) C. E. Wenner, *J. Cell Physiol.,* 2012, **227**, 450-456; (b) S. Fulda, L. Galluzzi and G. Kroemer, *Nat. Rev. Drug Discovery,* 2010, **9**, 447-464.

48 (a) J. S. Armstrong, *Br. J. Pharmacol.,* 2006, **147**, 239-248; (b) G. Damia, L. Imperatori, M. Stefanini and M. D'Incalci, *Int. J. Cancer,* 1996, **66**, 779-783.

49 A. Basu and S. Krishnamurthy, *J. Nucleic Acid,* 2010, Article ID 201367.

50 (a) S. Marrachea, S. Tundup, D. A. Harn and S. Dhar, *ACS Nano,* 2013, 7, 7392-7402; (b) S. Marrache, R. K. Pathak and S. Dhar, *Proc. Natl. Acad. Sci. USA,* 2014, **111**, 10444-10449.

51 (a) E. Delaey, F. V. Laar, D. D. Vos, A. Kamuhabwa, P. Jacobs and P. D. Witte, *J. Photochem. Photobiol. B,* 2000, **55**, 27-36; (b) J. Saczko, M. Mazurkiewicz, A. Chwilkowska, J. Kulbacka, G. Kramer, M. Ługowski, M. Śnietura and T. Banas, *Folia Biol. (Praha),* 2007, **53**, 7-12.

52 (a) I. Kostova, I. Manolov and G. Momekov, *Eur. J. Med. Chem.*, 2004, **39**, 765–775; (b) I. Kostova, N. Trendafilova and G. Momekov, *Eur. J. Med. Chem.,* 2005, **99**, 477-487.

53 K. Nakamoto, in *Infrared and Raman Spectra of Inorganic and Coordination Compounds*, John Wiley & Sons, New York, 3rd edn, 1978.

54 W. J. Geary, *Coord. Chem. Rev.,* 1971, **7**, 81-122.

55 J. C. G. Bünzli, A. E. Merbach and R. M. Nielson, *Inorg. Chim. Acta,* 1987, **139**, 151-152.

56 Y. Fukuda, A. Nakao and K. Hayashi, *J. Chem. Soc., Dalton Trans.,* 2002, 527-533.

57 A. Leonidova, V. Pierroz, R. Rubbiani, J. Heier, S. Ferrari and G. Gasser, *Dalton Trans.,* 2014, **43**, 4287-4294.

58 (a) S. Banerjee, A. Dixit, R. N. Shridharan, A. A. Karande and A. R. Chakravarty, *Chem. Commun.,* 2014, **50**, 5590-5592; (b) C. Qian, J. Q. Wang, C. L. Song, L. L. Wang, L. N. Ji and H. Chao, *Metallomics,* 2013, **5**, 844-854.

59 J. D. McGhee and P. H. von Hippel, *J. Mol. Biol.*, 1974, **86**, 469-489.

60 A. M. Angeles-Boza, P. M. Bradley, P. K.-L. Fu, S. E. Wicke, J. Bacsa, K. R. Dunbar and C. Turro, *Inorg. Chem.*, 2004, **43**, 8510-8519.

61 (a) Y. An, S.-D. Liu, S.-Y. Deng, L.-N. Ji and Z.-W. Mao, *J. Inorg. Biochem.*, 2006, **100**, 1586-1593; (b) L. E. Gunther and A. S. Yong, *J. Am. Chem. Soc.*, 1968, **90**, 7323-7328.

62 J. M. Veal and R. L. Rill, *Biochemistry*, 1991, **30**, 1132-1140.

63 P. P Pellegrini and J. R. Aldrich-Wright, *Dalton Trans*., 2003, 176-183.

64 S. Tobita, M. Arakawa and I. Tanaka, *J. Phys. Chem.*, 1984, **88**, 2697-2702.

65 T. Phillips, I. Haq, A. J. H. M. Meijer, H. Adams, I. Soutar, L. Swanson, M. J. Sykes and J. A. Thomas, *Biochemistry*, 2004, **43**, 13657-13665.

66 S. Delaney, M. Pascaly, P. K. Bhattacharya, K. Han and J. K. Barton, *Inorg. Chem.*, 2002, **41**, 1966-1974.

67 K. Szacilowski, W. Macyk, A. Drzewiecka-Matuszek, M. Brindell, and G. Stochel, *Chem. Rev*., 2005, **105**, 2647-2694.

68 (a) A. U. Khan, *J. Phys. Chem.*, 1976, **80**, 2219-2228; (b) P. B. Merkel and D. R. Kearns, *J. Am. Chem. Soc.*, 1972, **94**, 1029-1030.

69 (a) M. Tanaka, K. Ohkubo and S. Fukuzumi, *J. Phys. Chem. A*, 2006, **110**,11214-11218; (b) M. L. Cunningham, J. S. Johnson, S. M. Giovanazzi and M. J. Peak, *Photochem. Photobiol*., 1985, **42**, 125-128.

70 D. D. Perrin, W. L. F. Armarego and D. R. Perrin, *Purification of Laboratory Chemicals*; Pergamon Press: Oxford, **1980**.

71 O. Vajragupta, P. Boonchoon and L. J. Berliner, *Free Radicals Res.,* 2004, **38**, 303-314.

72 (a) E. C. Constable, A. J. Edwards, R. Martínez-Máñez, P. R. Raithby and A. M. W. C. Thompson, *J. Chem. Soc., Dalton Trans.,* 1994, 645-650; (b) S. A. Moya, R. Pastene, H. L. Bozec, P. J. Baricelli, A. J. Pardey and J. Gimeno, *Inorg. Chim. Acta,* 2001, **312**, 7-14.

73 J. Guilford II, R. Jackson, C. Choi and W. R. Bergmark, *J. Phys. Chem.,* 1985, **89**, 294-300.

74 J. R. Lakowicz in *Principles of Fluorescence Spectroscopy*, Kluwer Academic/Plenum Publishers, New York, **1999**.

75 A. T. R. Williams, S. A. Winfield and J. N. Miller, *Analyst,* 1983, **108**, 1067-1071.

76 N. Walker and D. Stuart, *Acta Crystallogr.,* 1983, **A39**, 158-166.

77 (a) G.M. Sheldrick, *Acta Crystallogr. Sect. A*, 2008, **64**, 112−122; (b) L. J. Farrugia, *J. Appl. Crystallogr*., 1999, **32**, 837-838.

78 C. K. Johnson, *ORTEP, Report ORNL-5138*; Oak Ridge National Laboratory: Oak Ridge, TN, **1976**.

79 (a) A. D. Becke, *Phys. Rev*., 1998, **A38**, 3098-3100; (b) A. D. Becke, *J. Chem. Phys*., 1993, **98**, 5648-5652; (c) C. Lee, W. Yang, R. G. Parr, *Phys. Rev. B*., 1988, **37**, 785-789

80 M. J. Frisch, G. W. Trucks, H. B. Schlegel, G. E. Scuseria, M. A. Robb, J. R. Cheeseman, J.A. Montgomery, T. Vreven, K. N. Kudin, J. C. Burant, J. M. Millam, S. S. Iyengar, J. Tomasi, V. Barone, B. Mennucci, M. Cossi, G. Scalmani, N. Rega, G. A. Petersson, H. Nakatsuji, M. Hada, M. Ehara, K. Toyota, R. Fukuda, J. Hasegawa, H. Ishida, T. Nakajima, Y. Honda, O. Kitao, H. Nakai, M. Klene, X. Li, J. E. Knox, H. P. Hratchian, J. B. Cross, C. Adamo, J. Jaramillo, R.Gomperts, R. E. Stratmann, O. Yazyev, A. J. Austin, R. Cammi, C. Pomelli, J. Ochterski, P. Y. Ayala, K. Morokuma, G. A. Voth, P. Salvador, J. J. Dannenberg, V. G. Zakrzewski, S.Dapprich, A. D. Daniels, M. C. Strain, O. Farkas, D. K. Malick, A. D. Rabuck, K. Raghavachari, J. B. Foresman, J. V. Ortiz, Q. Cui, A. G. Baboul, S. Clifford, J. Cioslowski, B. B. Stefanov, G. Liu, A. Liashenko, P. Piskorz, I. Komaromi, R. L. Martin, D. J. Fox, T. Keith, M. A. Al-Laham, C. Y. Peng, A. Nanayakkara, M. Challacombe, P. M. W. Gill, B. Johnson, W. Chen, M. W. Wong, C. Gonzalez and J. A. Pople, Gaussian 03, revision B.4; Gaussian Inc.: Pittsburgh, PA, **2003**.

81 (a) J. L. McClintock and B. P. Ceresa, *Invest. Opthalmol. Vis. Sci*., 2010, **51**, 3455-3461; (b) A. Bhattacharyya, A. Dixit, K. Mitra, S. Banerjee, A. A. Karande and A. R. Chakravarty, *MedChemComm*, 2015, **6**, 846–851.

82 T. Mosmann, *J. Immunol. Methods,* 1983, **65**, 55-63.

83 A. S. Keston and R. Brandt, *Anal. Biochem*., 1965, **11**, 1-5.

84 T. Takanashi, Y. Ogura, H. Taguchi, M. Hashizoe and Y. Honda, *Invest. Ophthalmol. Vis. Sci*., 1997, **38**, 2721-2728.

85 (a) S. Banerjee, A. Dixit, A. Kumar, S. Mukherjee, A. A. Karande and A. R. Chakravarty, *Eur. J. Inorg. Chem*., 2015, 3986–3990; (b) C. Soni and A. A. Karande, *Mol. Immunol*., 2010, **47**, 2458-2466.

86 M. E. Reichmann, S. A. Rice, C. A. Thomas and P. Doty, *J. Am. Chem. Soc.*, 1954, **76**, 3047-3053.

87 M. T. Carter, M. Rodriguez and A. J. Bard, *J. Am. Chem. Soc.*, 1989, **111**, 8901-8911.

88 J. Bernadou, G. Pratviel, F. Bennis, M. Girardet and B. Meunier, *Biochemistry*, 1989, **28**, 7268-7275.

Table 1. Selected physicochemical data for the complexes **1**–**4**.

Complex	ESI-MS (m/z)[a]	IR[b]/cm^{-1}			Λ_M[c] / S cm^2 mol^{-1}	Φ[d]	E_f/ V (ΔE_p/ mV)[e]	μ_{eff}[f]	K_b / M^{-1} [s][g]	ΔT_m[h] / °C
		NO_3^-	Olefinic C=C	C=O						
1	614.09	1383	1498	1590	85	-	-	3.62	3.0 (±0.1) 10^4 [0.1]	1.7
2	880.11	1390	1495	1592	71	0.02	-	3.56	9.2 (±0.2) 10^4 [0.2]	2.8
3	722.08	1380	1505	1596	82	-	0.61 (140)	3.58	2.1 (±0.2) 10^4 [0.1]	1.6
4	990.14	1388	1502	1602	69	0.02	0.61 (120)	3.60	7.8 (±0.3) 10^4 [0.2]	2.6

[a] The molecular ion peak arising from the $[M–(NO_3^-)]^+$ species in aqueous methanol. [b] Recorded on solid sample. [c] Molar conductivity in DMF at 25 °C. [d] Fluorescence quantum yield measured in DMF solution of the complex , excitation wavelength = 420 nm. [e] $E_f = 0.5\ (E_{pa} + E_{pc})$, $\Delta E_p = (E_{pc} - E_{pa})$, where E_{pa} and E_{pc} are the respective anodic and cathodic peak potentials (vs. SCE) for the Fc^+/Fc couple. [f] μ_{eff} in μ_B obtained by NMR method using DMSO-d_6 solutions of the complexes at 25 °C. [g] K_b, DNA binding constant (s, binding site size). [h] Change in the DNA melting temperature.

Table 2. Selected crystallographic data and structure refinement parameters for the complex **1**.

Empirical formula	$C_{26}H_{22}N_5O_8Nd$ (**1**)
Formula weight (gmol^{-1})	676.73
Crystal system	Triclinic
Space group	*P*-1
a (Å)	9.5473(5)
b (Å)	10.7596(6)
c (Å)	14.1625(8)
α (°)	77.029(2)
β (°)	81.295(2)
γ (°)	70.083(2)
V (Å^3)	1328.47(13)
Z	2
T (K)	293(2)
ρ_{calc} (g cm^{-3})	1.692
λ/Å (Mo-K_α)	0.71073
μ (mm^{-1})	2.013
Theta range for data collection	1.48 ° to 26.00 °
Reflections collected / unique	21812 / 5242
Data/restraints/parameters	5242/0/361
F(000)	674
Goodness-of-fit on F^2	1.056
R (F_o)[a], I>2σ(I) / wR (F_o)[b]	0.0236/0.0582
R (all data)/wR (all data)	0.0278/0.0599
Largest diff. peak and hole (e Å^{-3})	0.580, -0.348

[a] $R = \Sigma||F_o|-|F_c||/\Sigma|F_o|$. [b] $wR = \{\Sigma[w(F_o^2-F_c^2)^2]/\Sigma[w(F_o)^2]\}^{½}$; $w = [\sigma^2(F_o)^2 + (0.0345\ P)^2 + 0.2390P]^{-1}$, where $P = (F_o^2 + 2F_c^2)/3$.

Table 3: IC_{50} values of complexes **1-4** in HeLa and MCF-7 (in the parentheses) cell lines.[a]

Compound	Light / μM	Dark / μM
1	53.1±2.5	80.3± 2.1
	(62.6±2.8)	(94.5±3.1)
2	4.2±0.8	>50
	(9.6±1.2)	(>50)
3	13.2 ±1.6	>50
	(19.9±1.8)	(>50)
4	0.7± 0.2	>50
	(2.1±0.6)	(>50)
	(34.1±1.2)[b]	(>50)
Curcumin (Hcurc)[c]	8.2±0.2	85.4± 0.6
	(19.9±1.4)	(90.3±4.9)
Ph-tpy[d]	>100	>100
	(>100)	(>100)

[a] Light of 400-700 nm (10 J cm^{-2}) wavelength. [b] In MCF-10A cells. [c] Reference 43. [d] Reference 29. The photocytotoxicity of Fc-tpy ligand could not be measured due to its insolubility in the buffer medium (Reference 29).

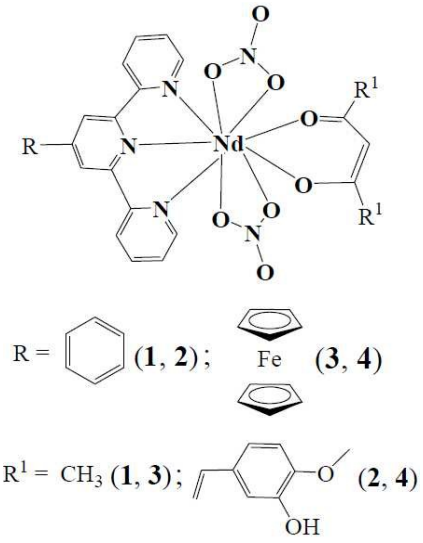

Fig.1 The schematic representation of the complexes **1**–**4**.

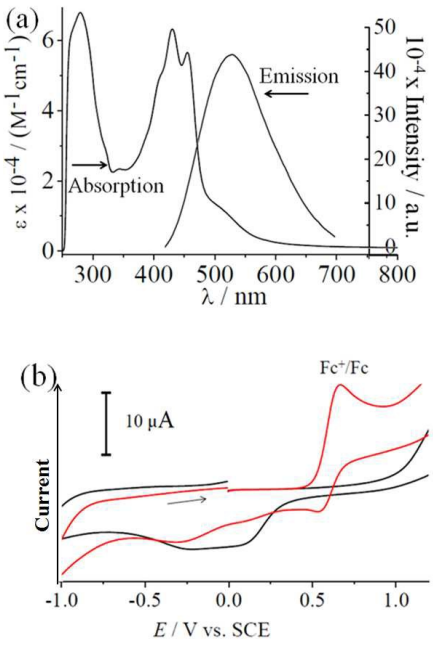

Fig. 2 (a) The electronic absorption spectrum in 5% aqueous DMF and the emission spectrum in DMF for complex **4** (excitation wavelength, 420 nm); (b) Cyclic voltammograms of complexes **2** (black curve) and **4** (red curve) recorded in DMF in the presence of 0.1 M TBAP as supporting electrolyte.

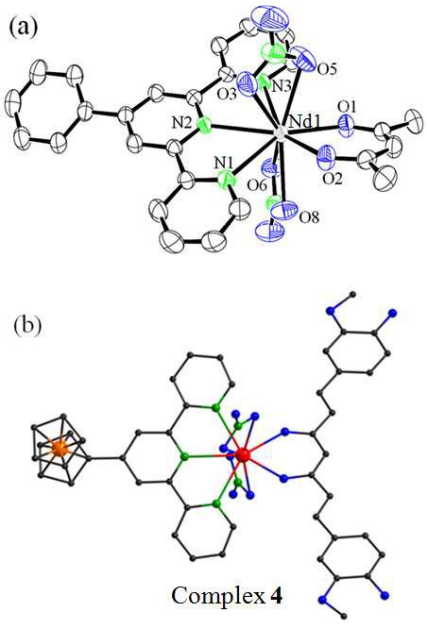

Fig. 3 (a) ORTEP diagram of the complex **1** drawn at 40% probability. The hydrogen atoms and the counter anions have been omitted for clarity. The color codes are: metal (light brown), nitrogen (green), oxygen (blue) and carbon (black); Nd(1)-O(1) = 2.3407(19); Nd(1)-O(2) = 2.3391(18); Nd(1)-N(1) = 2.578(2); Nd(1)-N(2) = 2.635(2); Nd(1)-N(3) = 2.607(2); Nd(1)-O(3) = 2.528(2); Nd(1)-O(5) = 2.566(2); Nd(1)-O(6) = 2.562(2); Nd(1)-O(8) = 2.566(2); (b) The DFT optimized structure of complex **4**. The structure was obtained by using B3LYP level theory and LanLD2Z basis set. The color codes are: metal (red), nitrogen (green), oxygen (blue) and carbon (black).

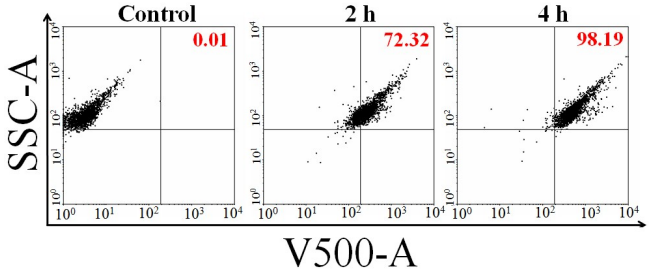

Fig. 4. Cellular uptake of complex **4** (1 μM) at 2 h and 4 h of incubation with HeLa cells as determined from the FACS analysis.

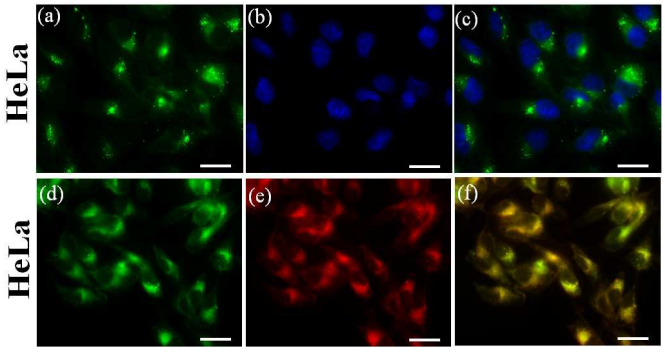

Fig. 5. Fluorescence microscopic images of the HeLa cancer cells treated with 30 μM of **4** on 4 h incubation and Hoechst 33342 dye (5 μg mL^{-1}): panel (a): emission from **4**; panel (b): blue emission from the nucleus staining Hoechst dye; panel (c): merged images showing cytosolic localization of **4**; panel (d): fluorescence emission from **4**; panel (e): red emission from the Mitotracker red (0.5 μM) dye. The scale bar: 20 μm.

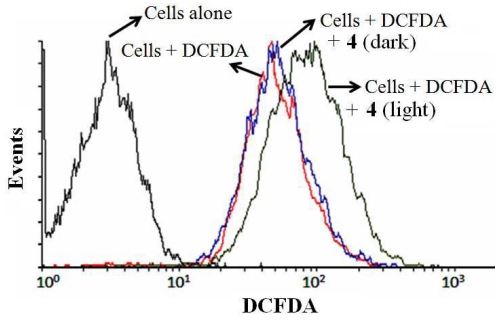

Fig. 6. DCFDA/DCF assay performed for the detection of ROS generation by complex **4** in HeLa cells. (Light source: visible light of 400–700 nm).

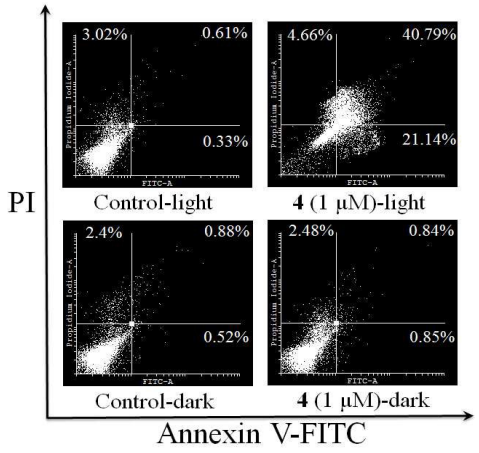

Fig. 7. Annexin V-FITC/PI coupled flow cytometry analysis showing complex **4** (3 μM) induced apoptosis in the presence of visible light (400–700 nm).

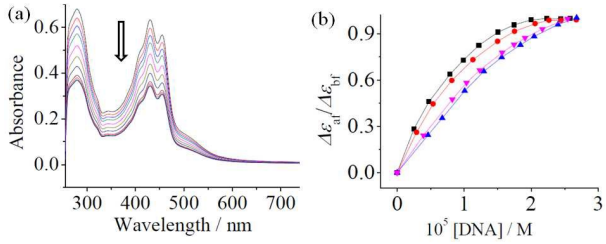

Fig. 8. (a) Plots showing the absorption spectral decrease of complex **4** in 5 mM Tris-HCl buffer (pH 7.2) on increasing the concentration of ct DNA; (b) The least-squares fit of $\Delta\varepsilon_{af}/\Delta\varepsilon_{bf}$ vs. [DNA] for complexes **1** (▲), **2** (●), **3** (■) and **4** (▼) to calculate K_b using MvH equation.

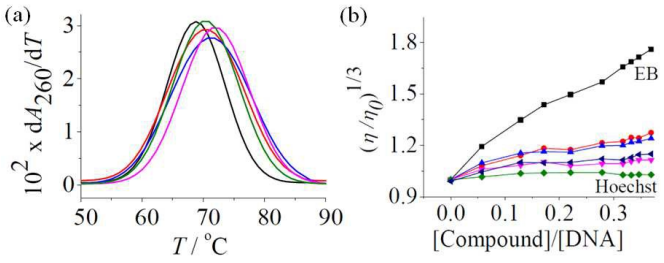

Fig. 9. (a) Melting plots of 200 μM ct DNA alone (black) and on addition of the complex **1**(green), **2** (pink), **3** (red), **4** (blue); (b) Effect of increasing the concentration of the complex **1**(▼), **2** (▲), **3** (◀), 4(●), ethidium bromide (EB, ■) and Hoechst 33258 (♦) on the relative viscosities of ct-DNA at 37.0 (± 0.1) °C in 5 mM Tris-HCl buffer (pH 7.2) containing 2.0 – 20% DMF, [DNA] = 150 μM.

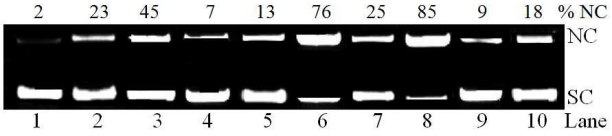

Fig. 10. Cleavage of SC pUC19 DNA (0.2 μg, 30 μM) by the complexes **1**–**4** (10 μM) in 50 mM Tris-HCl/NaCl buffer (pH, 7.2) on photo-irradiation at 454 nm (60 mW) for 2 h: lane 1, DNA control; lane 2, DNA + Hcurc (10 μM, dark); lane 3, DNA + Hcurc (10 μM); lane 4, DNA + **4** (10 μM, dark); lanes 5-8, DNA + complexes **1**–**4**, respectively; lane 9, DNA + distamycin-A (50 μM); lane 10, DNA + distamycin-A (50 μM) + **4**.

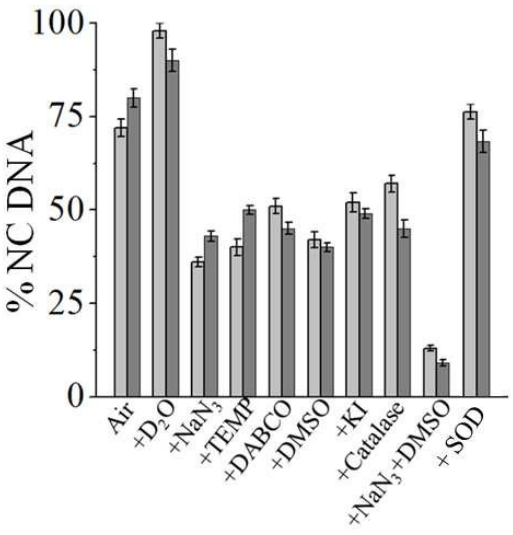

Fig. 11. Bar diagrammatic representation of the photocleavage of SC pUC19 DNA (0.2 μg, 30 μM) induced by complex **2** (light gray) and complex **4** (dark gray) in the presence of various additives in Tris-HCl buffer. The additive concentrations/quantities are: sodium azide, 0.5 mM; KI, 0.5 mM; TEMP, 0.5 mM; DABCO, 0.5 mM; D_2O, 16 μL; DMSO, 4 μL; catalase, 4 units; SOD, 4 units. Light source: visible light of 454 nm (60 mW).

Mitochondrial selectivity and remarkable photocytotoxicity of a ferrocenyl neodymium(III) complex of terpyridine and curcumin in cancer cells

Tukki Sarkar,[a] Samya Banerjee,*[b] Sanjoy Mukherjee [b] and Akhtar Hussain*[a]

Synopsis: Mixed-ligand neodymium(III) complex of ferrocene appended terpyridine and curcumin shows remarkable visible-light induced cytotoxicity in HeLa and MCF-7 cancer cells. The cell death is apoptotic in nature and triggered by the formation of ROS on photoirradiation. Fluorescence imaging studies reveal mitochondrial localization of the complex.

Keywords: Neodymium(III), Curcumin, Crystal Structure, Mitochondria, Photodynamic Therapy, Apoptosis

Running title. *"Mitochondrial selectivity and remarkable photocytotoxicity ..."*

Pictogram: